

## Supplemental Material

### Across-strike asymmetry of the Andes orogen linked to the age and geometry of the Nazca plate

Pedro Val<sup>1,2\*</sup>, Jane K. Willenbring<sup>1,3</sup>

<sup>1</sup> *Scripps Institution of Oceanography, University of California San Diego, La Jolla, CA 92093, USA.*

<sup>2</sup> *Now at Department of Geology, School of Mines, Federal University of Ouro Preto, Ouro Preto, MG, Brazil*

<sup>3</sup> *Now at Stanford University, Department of Geological Sciences, Stanford, CA 94305, USA*

\*Corresponding author: [pedroval07@gmail.com](mailto:pedroval07@gmail.com)

This Supplemental Material contains:

Supplemental Datasets S1, S2 (Attached Excel File), S3 and S4 (Attached PDFs).

Supplemental Text S1 and S2

Supplemental Table S1-S3 (Attached Excel File).

#### Supplemental Text S1 – Corrections to the retro-wedge limits

To define the retro-wedge limits of the orogenic wedge (i.e. the deformation front), we use the published geological map of South America (Gómez et al., 2019). However, we repositioned the retro-wedge limits in (i) Peru to include the Contaya, Moa, and Shira ranges based on previous studies (e.g. Dumont et al., 1991; Hermoza et al., 2005; Espurt et al., 2008) and (ii) southern Argentina to include both the San Rafael block and the Agrio fold and thrust belt based on previous studies (e.g. Folguera et al., 2007, 2009). In both cases, the retro-wedge limits are positioned east of the limits defined in Gómez et al. (2019). Basement uplifts are part of the Andean belt, reflect the accommodation of strain in the back-arc and are integral parts of the orogen evolution (Jordan et al. 1983). Including basement uplifts east of the deformation front is also a way of accounting for the inherited crustal heterogeneity that is thought to contribute to the evolution of the Andes (e.g. Kley et al., 1999), which we do not discuss in the main text.

#### Supplemental Text S2

In the multilinear models described in the main text, adjusting both  $Y$  and  $X_2$  to  $X_1$  can reveal the partial dependence of  $Y$  on  $X_2$ . This partial dependence can be represented in partial regression plots (Cook and Weisberg, 1984), which we only show coefficients for (Fig. 2 E-I). We also present the partial dependence as partial residual plots as shown in the main text (Fig. 2 J-M), which do not adjust  $X_2$  for  $X_1$  and are, therefore, useful to detect nonlinear behaviors (Larsen and McCleary, 1972). The regression trends presented in Fig. 2 J-M are obtained from the coefficients of the partial regressions. These coefficients were obtained by regressing the residuals of  $Y$  on  $X_1$  against the residuals of  $X_2$  on  $X_1$ .

#### Supplemental Text S3 – Erosion rate, topographic, and climatic data

From the 493 basins obtained from the Octopus database (<https://doi.org/10.5194/essd-10-2123-2018>), we exclude (i) replicates ( $n=65$ ), (ii) basins with drainage area greater than  $10^4$

km<sup>2</sup> and extending beyond the Andean deformation front (n = 39), (iii) basins with abnormally weak lithology (n=9), glacial activity (n=1), or spurious erosion rates (n=5). The same basins were used to obtain topographic and rainfall data. A drainage area threshold of 10<sup>6</sup> m<sup>2</sup> and 5 x 10<sup>5</sup> m<sup>2</sup> was used for the 90 m and 30 m resolution datasets, respectively.

In the orogen asymmetry analysis, we calculate the modal rainfall rates for the pro- and retro-wedge areas. We used the same swath profiles shown in Fig. 1 to obtain a 100-km wide rainfall rate data (red line in Fig. S1). A 40-bin histogram was then produced for each swath-profile and the pixels divided into pro-wedge and retro-wedge areas based on the position of the mean orogen peaks as described in the main text (Fig. S1). A smoothing kernel was then fit to the histogram for each side of the orogen. From the smoothed kernel, we obtain the peak, most prominent signal (see Fig. S2). A latitudinal plot of the inferred rainfall rates highlights the orographic effects along and across strike of the Andes along with the calculated orogenic wedge widths (Fig. S3). Rainfall rates, again, come from published datasets (Karger et al., 2018). Topographic profiles and rainfall histograms used in this study are provided as a Supplemental Dataset.

Lastly, subduction erosion could potentially affect the orogen asymmetries by decreasing the length of the pro-wedge and lowering the asymmetry values used in our analysis. Subduction erosion is on the order of 30 km over the last 20 Ma in the Central Andes where we mostly do not use in the orogen asymmetry analysis (Laursen et al., 2002; von Huene and Ranero, 2003; Clift and Hartley, 2007). Nonetheless, we applied a 30 km summation on the total wedge width and pro wedge width for the segment between 17°S and 32°S, where subduction erosion is the greatest and over the entire dataset. These corrections are imperceptible and do not change the statistics of our partial regression analysis (not shown).

# Supplemental Figures S1-S3:

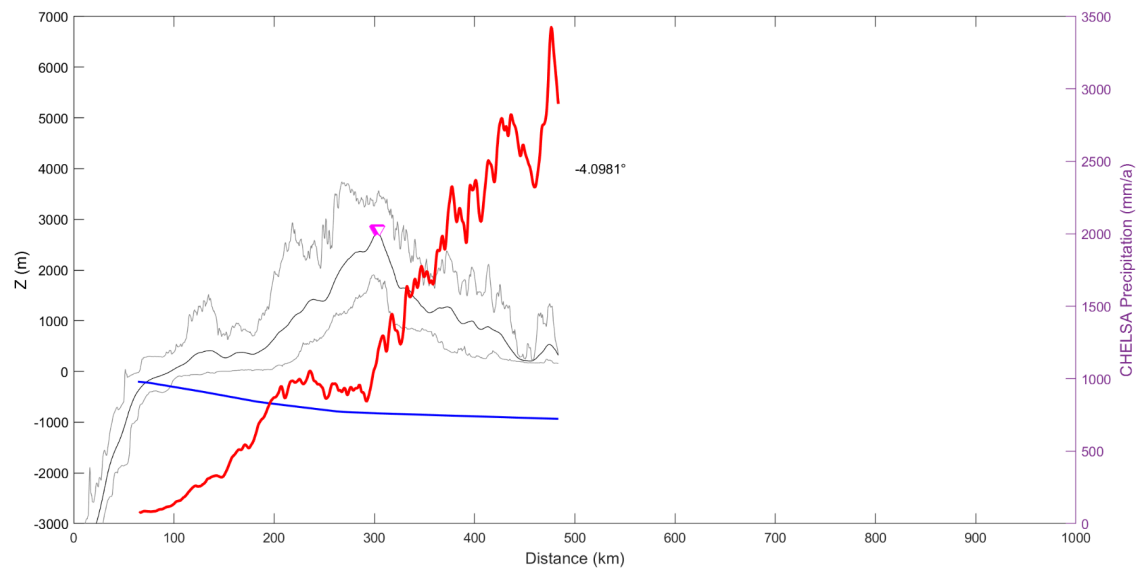


**Figure S1: Example of a swath profile used in this study.** The swath depicts the mean bathymetry and elevation (solid black line), the minimum and maximum traces (i.e. thin black line) obtained from the SRTM15+ dataset (Tozer et al., 2019). The mean elevation was smoothed with a 10 km moving mean before finding the highest 1% elevations (pink triangles). The blue line shows the profile of the subducted Nazca slab (with depth values in meters divided by 100 simply to represent the shape of the slab). The red line shows the precipitation profile in mm/a (right Y-axis). The total distance of the figure is kept at 1000 km to allow an intuitive comparison with the other profiles.

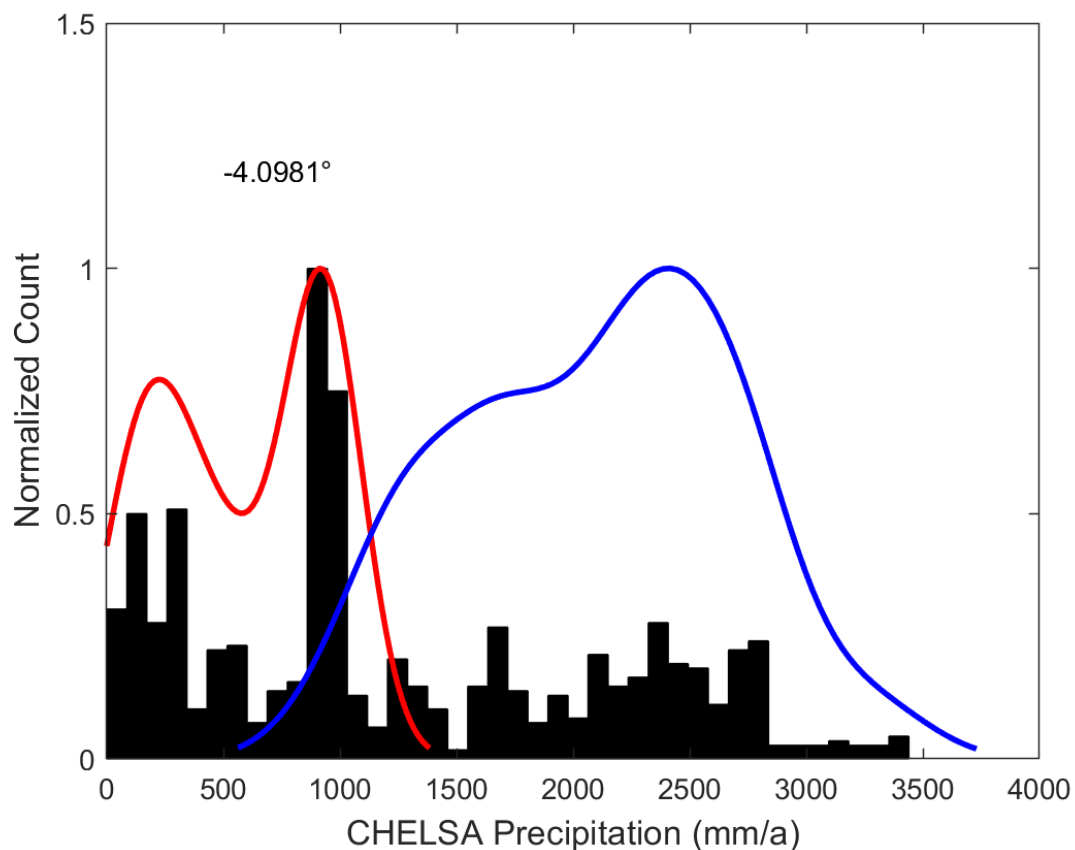


**Figure S2: Example of a rainfall rate histogram used to calculate modal precipitation.** Kernel functions are fit to the histograms individually for the pro-wedge (red) and retro-wedge rainfall rates (blue). All histograms are provided as Supplemental Dataset.

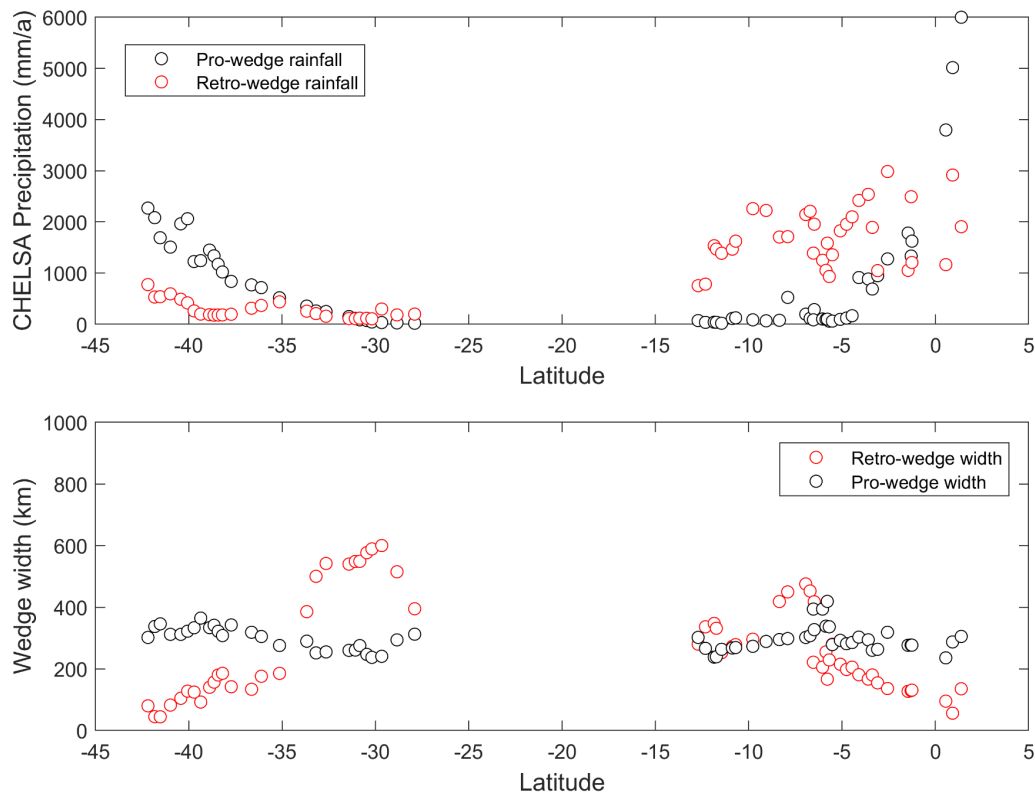


**Figure S3: Latitudinal distribution of calculated modal rainfall rates (top) and wedge widths (bottom).**

## References Cited

- Clift, P.D., and Hartley, A.J., 2007, Slow rates of subduction erosion and coastal underplating along the Andean margin of Chile and Peru: *Geology*, v. 35, p. 503–506, doi:10.1130/G23584A.1.
- Cook, R. D., & Weisberg, S., 1982, *Residuals and influence in regression*: New York, Chapman and Hall, 230 p.
- Dumont, J.F., Deza, E. and Garcia, F., 1991, Morphostructural provinces and neotectonics in the Amazonian lowlands of Peru: *Journal of South American Earth Sciences*, 4(4), p. 373–381, doi: 10.1016/0895-9811(91)90008-9
- Espurt, N., Brusset, S., Baby, P., Hermoza, W., Bolaños, R., Uyen, D. and Déramond, J., 2008. Paleozoic structural controls on shortening transfer in the Subandean foreland thrust system, Ene and southern Ucayali basins, Peru: *Tectonics*, 27(3), doi: 10.1029/2007TC002238
- Folguera, A., Introcaso, A., Giménez, M., Ruiz, F., Martinez, P., Tunstall, C., Morabito, E.G. and Ramos, V.A., 2007, Crustal attenuation in the Southern Andean retroarc (38–39 30'

- S) determined from tectonic and gravimetric studies: the Lonco-Luán asthenospheric anomaly: *Tectonophysics*, v. 439(1-4), p.129-147, doi: 10.1016/j.tecto.2007.04.001
- Folguera, A., Naranjo, J.A., Orihashi, Y., Sumino, H., Nagao, K., Polanco, E., and Ramos, V. A., 2009, Retroarc volcanism in the northern San Rafael Block (34–35 30' S), southern Central Andes: occurrence, age, and tectonic setting: *Journal of Volcanology and Geothermal Research*, v. 186(3-4), p. 169-185, doi: 10.1016/j.jvolgeores.2009.06.012.
- Gómez, J, Schobbenhaus, C. & Montes, N E., compilers 2019, Geological Map of South America 2018 Scale 1:5,000,000. Commission for the Geological Map of the World (CGMW), Colombian Geological Survey and Geological Survey of Brazil.
- Hermoza, W., Brusset, S., Baby, P., Gil, W., Roddaz, M., Guerrero, N. and Bolaños, R., 2005. The Huallaga foreland basin evolution: Thrust propagation in a deltaic environment, northern Peruvian Andes: *Journal of South American Earth Sciences*, v. 19(1), p. 21-34, doi: 10.1016/j.jsames.2004.06.005
- Jordan, T.E., Isacks, B., Allmendinger, R.W., Brewer, J.A., Ramos, V.A., and Ando, C.J., 1983, Andean tectonics related to geometry of subducted Nazca Plate: *Geological Society of America Bulletin*, v. 95, p. 877–880, doi:10.1130/0016-7606(1983)94<341:ATRTGO>2.0.CO;2.
- Karger, D.N., Conrad, O., Böhner, J., Kawohl, T., Kreft, H., Soria-Auza, R.W., Zimmermann, N.E., Linder, P., Kessler, M., 2017, Climatologies at high resolution for the Earth land surface areas: *Scientific Data*, v. 4, 170122, doi:10.1038/sdata.2017.122
- Kley, J., Monaldi, C.R., & Salfity, J.A., 1999, Along-strike segmentation of the Andean foreland: causes and consequences: *Tectonophysics*, v. 301(1-2), p. 75-94, 10.1016/S0040-1951(98)90223-2.
- von Huene, R., and Ranero, C.R., 2003, Subduction erosion and basal friction along the sediment-starved convergent margin off Antofagasta, Chile: *Journal of Geophysical Research*, v. 108, p. 2079, doi:10.1029/2001JB001569.
- Laursen, J., Scholl, D.W., and Huene, R. von, 2002, Neotectonic deformation of the central Chile margin: Deepwater forearc basin formation in response to hot spot ridge and seamount subduction: *Tectonics*, v. 21, p. 1–27, doi:10.1029/2001TC901023.